A molecular dynamics study to determine the solid-liquid interfacial tension using test area simulation method (TASM)

Anjan R. Nair and Sarith P. Sathian

Citation: J. Chem. Phys. **137**, 084702 (2012); doi: 10.1063/1.4746750
View online: http://dx.doi.org/10.1063/1.4746750
View Table of Contents: http://jcp.aip.org/resource/1/JCPSA6/v137/i8
Published by the American Institute of Physics.

A molecular dynamics study to determine the solid-liquid interfacial tension using test area simulation method (TASM)

Anjan R. Nair and Sarith P. Sathian[a)]
Computational Nanotechnology Lab, School of Nano Science and Technology, National Institute of Technology-Calicut, Kozhikode 673601, India

(Received 2 May 2012; accepted 3 August 2012; published online 23 August 2012)

Molecular dynamics (MD) studies on heat transfer from a heated nanoparticle into the surrounding fluid have indicated that the fluid next to a spherical nanoparticle can get heated well above its boiling point without observing a phase change, while a contradicting behavior was observed for a flat surface-fluid interface. Another interesting observation is that the critical heat flux was found to increase with increase in the wetting characteristics of solid. Thus, the interfacial tension or free energy of solid-liquid interface could play a pivotal role in the mechanism of heat transfer. A recent study by Gloor *et al.* [J. Chem. Phys. **123**, 134703 (2005)] has proposed test area simulation method (TASM) for the determination of interfacial tension. The present study involves the determination and the comparison of solid-liquid interfacial tension for planar and spherical interfaces using MD based on TASM and analyze the results. A higher interfacial tension value is observed for spherical nanoparticle fluid interface compared to flat surface fluid interface. The results also indicate that the solid-liquid interfacial tension is a size and temperature dependent property. The results from this study are also expected to give better insights into the possible reasons for the observed differences in the thermal transport for spherical nanoparticle-liquid interface compared to planar-liquid interface.
 [http://dx.doi.org/10.1063/1.4746750]

I. INTRODUCTION

Transport of heat energy at the solid-fluid interface is of considerable interest in the analysis of heat transfer in a variety of applications. However, the exact physical mechanism of heat transport while the fluid is in close contact with the solid is still not fully understood. There have been many experimental studies on the measurement of forces and transport of energy across planar solid-liquid interfaces at the nanoscale level.[1–4] Effects such as layering of liquid molecules adjacent to the solid surface, surface curvature, size effect, interactions in confined regions, effect of discontinuous potentials, hydrophobicity, etc., may add to the complexity of the problem.[5,6] Recent interest in many nanotechnological applications involving heat transfer at interfaces demand more insight into the physical mechanisms involved.

MD studies on planar gold surface and water interface have indicated that water layers get overheated and undergo explosive boiling. Repeated analysis with varying thickness of water layers also showed similar results.[7,8] However, theoretical simulations have demonstrated that the fluid surrounding a nanoparticle can be heated well above its boiling point without observing the occurrence of a phase change.[9]

The solid-liquid interface for a fluid-nanoparticle system and a fluid-planar surface has been further analyzed using MD.[10] For different heat inputs, the formation of vapor near the planar solid surface was observed, while the fluid next to the nanoparticle remained in the liquid state. Using a non-thermal equilibrium model, a higher critical heat flux value was reported for a spherical nanoparticle interface compared to a flat surface. This increased value of flux, which is required for the liquid to undergo boiling, was found to be increasing with wetting. Simulation studies of heated gold nanoparticle suspended in water and octane showed that the fluids are able to remain at liquid state even at high heat flux without undergoing an expected phase change. The effect of curvature of the interface on the interfacial tension, which inhibits the formation of an insulating vapor film was suggested as a reason for this phenomena.[9] The above studies suggest that the solid-liquid interfacial tension could play a pivotal role in the interfacial heat transfer. Accurate determination of the interfacial tension thus becomes important.

A common method[11–13] for estimating interfacial tension, which involves a mechanical route, requires the calculation of tensorial component of pressure. In the case of a planar interface, Kirkwood *et al.*[14] proposed a method which is well described by following equation:

$$\gamma = \int_{-\infty}^{\infty} [P_N(z) - P_T(z)]dz, \tag{1}$$

where γ is the interfacial tension, $P_N(z)$ and $P_T(z)$ are the normal and tangential components of pressure. Thus, this methodology involves the computation of components of pressure tensor as a function of the distance from the interface. The tensorial components of pressure are related to the derivative of intermolecular potential to give an explicit expression for interfacial tension.

The mechanical approach suffers from major disadvantages while applied to systems consisting of molecules interacting through discontinuous intermolecular potentials and non-planar interfaces. The pressure tensor could be difficult to

a)Electronic mail: sarith@nitc.ac.in. URL: http://www.cntl.nano.nitc.ac.in.

be evaluated for discontinuous potentials as well as for non-planar interfaces.

The second method of determining interfacial tension is based on finite size scaling method developed by Binder.[15] This involves estimating a Landau free energy barrier between coexisting phases from a simulation of the density of states. The method is computationally intensive and it is difficult to compute the values of density dependent free energy at low temperatures.

The third approach involves calculating the thermodynamic free energy difference between two systems to estimate the interfacial tension. According to the thermodynamic definition, interfacial tension is defined as the isothermal work of formation per unit area of interface.[16] Following the standard thermodynamic relation for a change in the Helmholtz free energy (F) for constant temperature (T), volume (V), and number of particles (N), the interfacial tension for planar interfaces[17] can be defined as

$$\gamma = \left(\frac{\partial F}{\partial A}\right)_{NVT}. \tag{2}$$

The right hand side of the above relation shows the change in free energy for an infinitesimal change in the interfacial area. Based on this free energy method, Gloor *et al.*[18] proposed test area simulation method (TASM), which calculates free energy affected by slight perturbation of the reference system. Details of this method are explained in Sec. II. It is interesting to note that there are other different methods based on the thermodynamic definition. Errington and Kofke[19] have presented a detailed study on these techniques.

Free-energy difference method requires two or more simulations to estimate the interfacial tension, which indicates the computational intensity of the method. However, the advantage of this test-area method is that it is very simple, and easier to implement. The generality of this technique in terms of applications compared to other two methods makes it a more acceptable method. Though TASM has been widely used by many researchers for determining interfacial (surface) tension of liquid vapor systems,[20–22] studies on solid-liquid interface leading to the analysis of heat transfer have been very limited. Bahadur *et al.*[21,22] performed an investigation to understand the effect of particle size on surface tension (liquid-vapor) and on deliquescence of saline water using MD simulation of NaCl-water vapor system. Mittal and Hummer[23] studied the effect of surface roughness on the interfacial free energy of water confined between two solid surfaces, using the mechanical approach proposed by Kirkwood.[14]

The primary motive of the present work is to explore the differences between solid-liquid interactions for planar and spherical interfaces. Molecular dynamics simulation was utilized for the determination of the interfacial tension between solid-fluid interfaces using TASM. The model system used for the simulation consists of monoatomic Lennard-Jones (LJ) solid and LJ liquid molecules. Interfacial tension was calculated for vapor-liquid and solid-liquid systems. A study on the effect of nanoparticle size and temperature on the interfacial tension was also performed. The results from this study are also expected to give better insights into the possible reasons for the observed differences in the thermal transport for spherical nanoparticle-liquid interface compared to a planar-liquid interface.

II. METHODOLOGY – TASM

In this method, change in free energy was evaluated from the perturbation of the systems without affecting properties of reference system. Solid-liquid interfacial tension (γ_{sl}) is thus measured by estimating the change in free energy for an infinestimal change in area. (Eq. (2)).

Finite difference techniques such as forward, backward, and central difference (CD) can be used for calculating this derivative (Eq. (2)). The use of a CD approximation not only improves the accuracy of the computed surface tension, but also allows one to circumvent the problem associated with an asymmetry in the free-energy differences, which is inherent in systems of particles interacting through discontinuous potentials. For implementing the test-area method using central difference method, three simulation cells are required, each constructed with an equal number of molecules, but different surface areas. The first step of this method is to simulate a system equilibrated to a reference state system 0 with interfacial area A_0. A test-area change is then performed to generate two perturbed state systems such that $A_1 = A_0(1+\Delta A)$ and $A_2 = A_0(1-\Delta A)$ keeping overall volume of the system as constant. Gloor *et al.*[18] has suggested a value of $\Delta A/A = \pm 0.0005$ for the relative perturbation in the area of the interface for systems with continuous potential and ± 0.0001 for square well potentials. Central difference approximation for the interfacial tension can be written as

$$\gamma = \left(\frac{\partial F}{\partial A}\right)_{CD} = \frac{f(F_0 + \Delta F) - f(F_0 - \Delta F)}{2\Delta A}. \tag{3}$$

The implementation of the method involves two independent perturbations: one in which the area of the interface A increases to $A+\Delta A$, and the other one, in which A decreases to $A-\Delta A$. For the changes in configurational energy of these perturbations denoted by $\Delta U^+ = U(A+\Delta A) - U(A)$ and $\Delta U^- = U(A-\Delta A) - U(A)$, respectively, Gloor *et al.*[18] have proved that the interfacial tension can be obtained from the expression as follows:

$$\gamma = \lim_{\Delta A \to 0} \frac{-kT}{2\Delta A}\left(\ln\left\langle \exp\left(-\frac{\Delta U^+}{kT}\right)\right\rangle - \ln\left\langle \exp\left(\frac{\Delta U^-}{kT}\right)\right\rangle\right). \tag{4}$$

III. MOLECULAR DYNAMICS SIMULATIONS AND RESULTS

In this section, the methodology used to estimate the interfacial tension is discussed. The method is implemented for (a) vapor-liquid planar interface (b) solid-liquid planar interface, and (c) solid-liquid spherical interface. The details of simulation and results of interfacial tension for each case are presented.

Table I shows the various dimensionless parameters used in this study. N is the number of particles, V is the volume, L, H represents the length and height of the simulation box,

TABLE I. Dimensionless parameters used in the study.

Property	Symbol	Dimensionless form
Height	z*	z/σ
Density	ρ^*	$N\sigma^3/v$
Temperature	T*	kT/ε
Interfacial tension	γ^*	$\gamma\varepsilon/\sigma^2$
Radial distance	r*	r/σ
Diameter	d*	d/σ
Time	t*	$(\sqrt{\varepsilon/m\sigma^2})t$

σ is the diameter of the particle, and ε is the well depth of LJ potential.[24]

A. Vapour liquid planar interface

1. Determination of coexistence density and critical point

In order to estimate the solid-liquid interfacial tension it is important to know the properties of the fluid such as critical point parameters (T_c^*,ρ_c^*) and surface tension when the liquid is in contact with the solid. Hence, for this purpose a monatomic LJ fluid characterized by diameter (σ) of the particle and the well depth (ε) of LJ potential was used for the study. Cut-off radius was taken as $r_c = 2.5\sigma$, since this was found to provide fairly accurate results as reported.[18]

The simulation was initiated from a face centered cubic (fcc) lattice in a cubic box. The temperature and overall number density ρ^* was chosen to be well within the gas-liquid coexistence condition based on the works by Finn *et al.*[25] and Smit.[26] These studies are based on the modification of the equation of state (EOS) data (p_{LJ}^*) of Nicolas *et al.*[27] for the full Lennard-Jones potential and have corrected the equation for the discontinuity at r_c by using the relation,

$$p_{tr}^*(T,\rho) = p_{\mathrm{LJ}}^*(T,\rho) + (8/3)\pi\rho^{*2}r_c^{*-3}, \quad (5)$$

where p_{tr}^* is the pressure of the Lennard-Jones fluid with truncated potential.

After the equilibration period of this homogeneous phase, two empty cubic cells of the same dimensions were added to both sides of the film in the z-direction, such that the dimensions of the simulation box was $z = 3x = 3y$, with periodic boundary conditions in all directions.[28–31] Then another equilibration stage of this system was achieved using *NVT* ensemble, during which the liquid vaporizes into the vacuum to form a stable two-phase system. The temperature was kept constant during the simulation by using a Nosé-Hover thermostat.[32,33] After the interfacial system was equilibrated, the production period was performed during which the liquid-gas coexisting densities and the surface tension values were evaluated.

TABLE II. Comparison of orthobaric densities obtained from present simulations with other works.

	Present work		Smit (Ref. 26)		Wilding (Ref. 34)	
T*	ρ_{liq}^*	ρ_{gas}^*	ρ_{liq}^*	ρ_{gas}^*	ρ_{liq}^*	ρ_{gas}^*
0.70	0.8289	0.0079	0.8201	0.0071	...	...
0.90	0.6923	0.0226	0.6845	0.0204	0.7197	0.0237
1.00	0.6498	0.0521	0.6447	0.0499	0.6668	0.0588
1.10	0.5764	0.1004	0.5743	0.0960	0.5611	0.1046

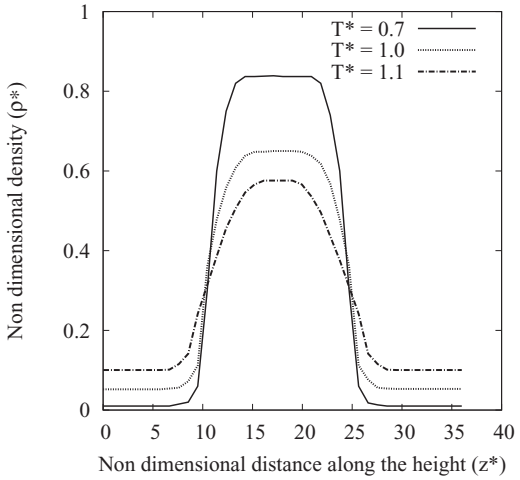

FIG. 1. Density profile of the liquid gas interface for different temperatures.

The coexisting densities were obtained by determining the density profile along the z-axis of the simulation box. Figure 1 shows the density profile (ρ^*) for the vapor liquid interface at various temperatures. The density profile $\rho(z)$ is computed at each temperature by averaging the histogram of densities in the z axis. The symmetrical nature of the density profile indicates that the system is properly equilibrated and also that a finite interfacial region is established.

Table II shows a comparison of the densities of liquid (ρ_{liq}) and gas (ρ_{gas}) phase obtained in the present study with the results of three important studies by Finn *et al.*,[25] Smit,[26] and Wilding[34] using Gibbs ensemble Monte Carlo (GEMC) method. It is to be noted that the cut off radius $r_c = 2.5\sigma$ was used for these works.

The gas-liquid phase boundary obtained from the simulations is shown in Fig. 2. Based on the law of rectilinear

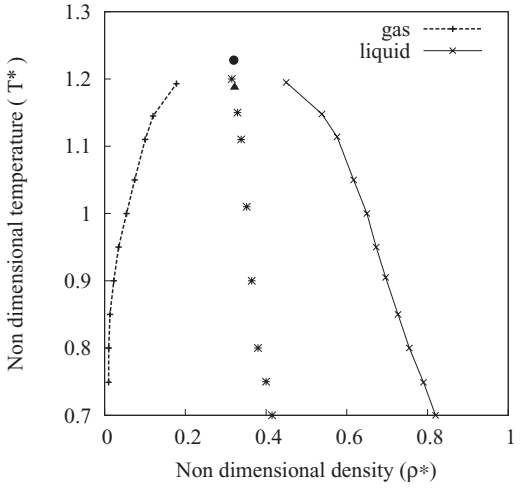

FIG. 2. Coexistence density profile of LJ fluid. The critical points based on works by • – Finn and Monson Ref. 25, ▲ – Wilding Ref. 34, * – average density of the coexisting phase.

diameters $(\rho_{gas} + \rho_{liquid})/2 = aT + b$, for the average density, the coefficient values, a = −0.18 and b = 0.53 were obtained from the present simulation results.

Determination of the critical point is the next crucial step. Nicolas *et al.*[27] have approximately estimated the critical parameters as $T_c^* = 1.35$ and $\rho_c^* = 0.35$ by using the EOS method, while Finn *et al.*[25] have estimated it as $T_c^* = 1.23$ and $\rho_c^* = 0.32$ by including a correction term for the truncation in the EOS.

However, studies on LJ fluids have shown that systematic size effects become apparent for $T^* = 0.95T_c^*$. Due to the influence of these finite size effects, any attempt to extrapolate the power law fit of density data near the critical point may lead to overestimating of the critical temperature.[35,36] To locate the exact critical point, a finite size scaling of the apparent critical temperature and density has been employed in many previous studies. This involves evaluating the critical temperature and density as

$$T_c^*(\infty) - T_c^*(L) \sim L^{-(\theta+1)/\upsilon}, \tag{6}$$

$$\langle\rho\rangle_c(L) - \langle\rho\rangle_c(\infty) \sim L^{-(d-1)/\upsilon}, \tag{7}$$

where L is the length of the simulation box, d = 3, $\theta = 0.54$, and $\upsilon = 0.629$.[34,37,38] Using the above relations, and based on GEMC method, Wilding[34] has determined the critical point for LJ fluid with $r_c = 2.5\sigma$ as $T_c^* = 1.1876$ and $\rho_c^* = 0.322$, while Panagiotopoulos[37] have reported $T_c^* = 1.176$ and $\rho_c^* = 0.33$, and for full potential (untruncated), $T_c^* = 1.312$ and $\rho_c^* = 0.316$ were obtained.[38] These values were estimated by linearly extrapolating the results at finite system lengths using corresponding temperature and density correlation length exponents.

Since the interfacial thickness ξ is associated with the correlation length[31] and becomes longer as temperature T* approaches critical point ($T \to T_c$, $\xi \to \infty$), the variation of ξ with temperature was also investigated. This thickness is estimated by fitting the final density obtained during the simulation (Fig. 1) to the following expression:[17]

$$\rho(z) = \frac{\rho_{liq} - \rho_{gas}}{2} - \frac{(\rho_{liq} - \rho_{gas})}{2}\tanh[2(z - z_0)/\xi], \tag{8}$$

where ρ_{liq}, ρ_{gas} are the densities of liquid and gas, and z_0 is the location of the equimolar dividing surface, where the density becomes the average of bulk gas and bulk liquid densities.

In this work, for temperatures between 0.7 and 1.05, the interfacial thickness varies from 0.06 to 0.14 times the x-dimension length (L_x). While at T* = 1.1 and 1.20 the thickness becomes approximately 0.45 times and 0.8 times L_x, respectively. When $\xi \approx$ L, finite size effects begin to dominate, hence for the present MD analysis, the critical temperature T_c^* could be closer to 1.23 as obtained by Finn and Monson.[25]

2. Determination of surface tension (γ_{vl}*)

The determination of surface tension or liquid-vapor interfacial tension was performed using an *NVT* ensemble in a simulation cell with the same dimensions as in Sec. III A 1.

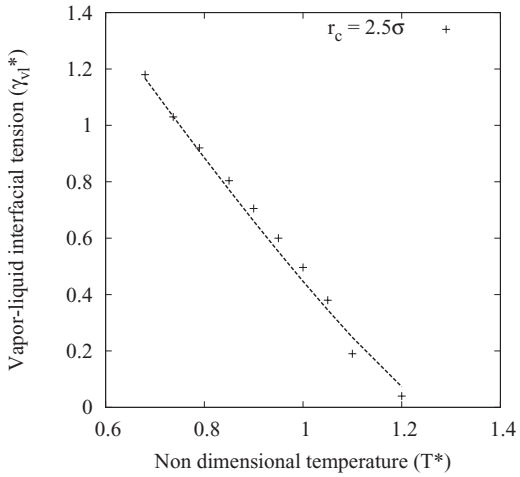

FIG. 3. Variation of vapor-liquid interfacial tension (γ_{vl}) with temperature.

Based on TASM method an infinestimal area change is applied and the dimension in the z-direction was altered keeping the overall volume and number of atoms constant in both the cases. Simulations are carried out for a total of 1×10^6 steps, each with $\Delta t^* = 0.005$. The configurational energy is recorded at every 5000 steps. Interfacial tension was calculated using the central difference formula (Eq. (4)). It is observed that the value of interfacial tension (γ_{vl}*) tends to decrease with increase in temperature (T*) (Fig. 3). The relation between the interfacial tension (γ) and critical temperature (T_c^*) can also be obtained from the Guggenheim corresponding states law,[17,39]

From the Guggenheim corresponding states law, the relation between the interfacial tension (γ) and critical temperature (T_c^*) can be obtained as

$$\gamma = \gamma_0(1 - T/T_c)^{\mu}, \tag{9}$$

where μ and γ_0 are the mean field theory exponent and "zero temperature" surface tension, respectively. The best optimal fit to the data from the present work (shown in Fig. 3) was obtained with a $\gamma_0 = 2.36 \pm 0.01$, Guggenheim mean field critical exponent[39] $\mu = 11/9$ and critical temperature $T_c = 1.23$.[25] Thus for the present study, critical temperature could be considered as $T_c^* = 1.23$ which is slightly higher compared to the critical values obtained by Wilding[34] and Panagiotopoulos[37] for a LJ fluid with $r_c = 2.5\sigma$.

B. Solid liquid interface

Following TASM and using the methods of calculations similar to the previous case, the solid-liquid interfacial tension is determined. Two cases were considered: liquids interfacing with planar surfaces and also with a spherical-nanoparticle. The fluid used is same as in preceding study of vapor liquid system. The fluid is assumed to be stationary and in thermal equilibrium with the walls. The system is maintained in thermodynamic equilibrium by keeping the fluid stationary and also maintaining the solid and liquid at thermal equilibrium.

The solid is modeled as monoatomic with LJ interaction. Separate simulations were carried out to ensure that melting

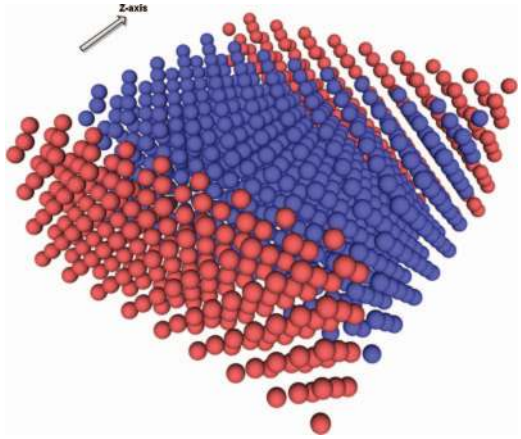

FIG. 4. Fluid enclosed between two solid walls.

of solid atoms (disintegration of atoms) did not occur for the temperature range specified in this work. The solid liquid interaction is also described by LJ potential which is expressed in terms of ratio $\varepsilon_r = \varepsilon_{sl}/\varepsilon_{ll}$ (ratio of solid liquid interaction potential (ε_{sl}) by liquid-liquid interaction potential (ε_{ll})). Three different values of ε_r were used : 0.30, 0.54, and 0.90. The atomic diameters of the liquid (σ_l) and solid particles (σ_s) is fixed as $\sigma_s = 0.75\sigma_l$.

1. Planar surface-liquid interface

Previous studies have shown that fluid on a thin planar surface tend to undergo explosive boiling upon subjected to heat transfer. The simulation model used for the present study is shown in Fig. 4. The fluid (blue colored) is enclosed between two solid atom walls (red colored) and the interfacial tension between the solid and the liquid is calculated. As stated in Sec. III B, the results for all γ_{sl}* values are calculated for "isothermal" solid-liquid interface.

The density profile of the fluid enclosed is shown in Fig. 5. The density reaches a peak value and gradually decays to a value corresponding to the bulk density at the mid section of the channel.

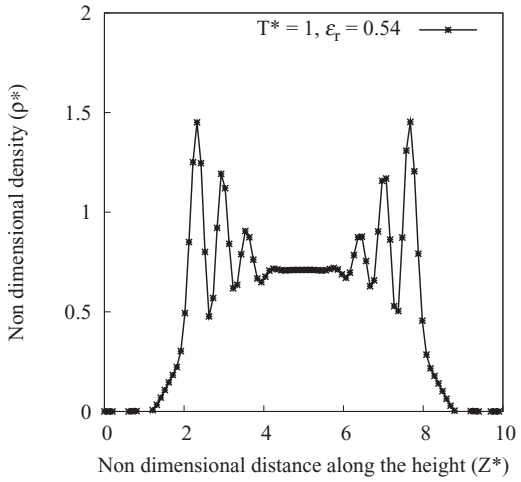

FIG. 5. Density profile of the liquid enclosed between two solid walls for T*=1.

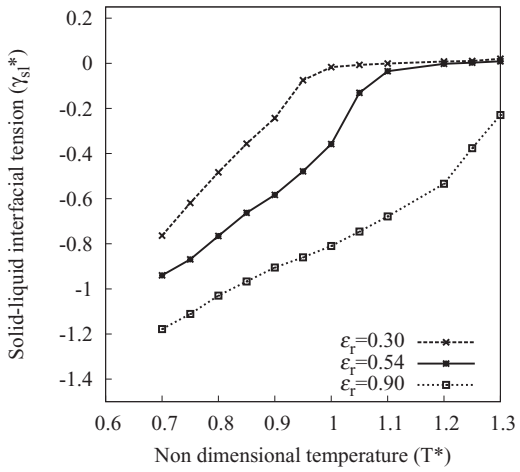

FIG. 6. Variation in solid-liquid interfacial tension (γ_{sl}*) for flat interface for different ε_r values.

Figure 6 shows the variation of solid-liquid interfacial tension γ_{sl}* with temperature for three ε_r values. The interfacial tension was determined for (001) crystallographic plane. It is observed that the value of (γ_{sl}*) decreases as temperature T* increases. Also there is a decrease in magnitude with reduction in ε_r. Similar to the trend observed in surface tension (γ_{vl}*) it can be noted that at around T* = 1.1 the curve becomes steeper. For the lower ε_r the curve becomes nonlinear and reaches zero at T* = 1.23 for $\varepsilon_r = 0.54$ and T* = 1.05 for $\varepsilon_r = 0.30$. This shows as ε_r reduces, the onset of nonlinearity also appears early. A zero value indicates the absence of liquid layer. It is interesting to note that, even at T* = 1.3, γ_{sl}* is not zero, indicating that a liquid layer is still adhering on the solid surface.

For a better understanding of the phenomenon, the contact angle model using the Young's equation (Eq. (10)) based on mechanical equilibrium was used to determine the contact or wetting angle (θ) of the fluid on the solid wall used in this study,

$$cos\theta = \frac{\gamma_{sv} - \gamma_{sl}}{\gamma_{vl}}. \tag{10}$$

Assuming the solid-vapor interfacial tension (γ_{sv}) as negligible ($\gamma_{sv} \approx 0$), the wetting angle was calculated at different temperatures. Figure 7 shows the variation of wetting angle with temperature. It is observed from Fig. 7 that wetting angle (θ) value increases as temperature increases for $\varepsilon_r = 0.30$ and 0.54, indicating that solid-fluid system undergoes a transition from wetting condition to non-wetting as temperature increases.

The results from the present study is compared with the results of an experimental study reported by Kandlikar and Steinke.[40] It is to be noted that they have measured the contact angle of water on heated surfaces. In addition, the variation of contact angle by using different materials and also by varying the surface roughness of the materials was measured. Although the fluid and solid wall in the present study are in thermal equilibrium, (for $\varepsilon_r = 0.30$ and 0.54 and temperatures below T* = 1.2), results from the present study are in good agreement with the their experiments.[40]

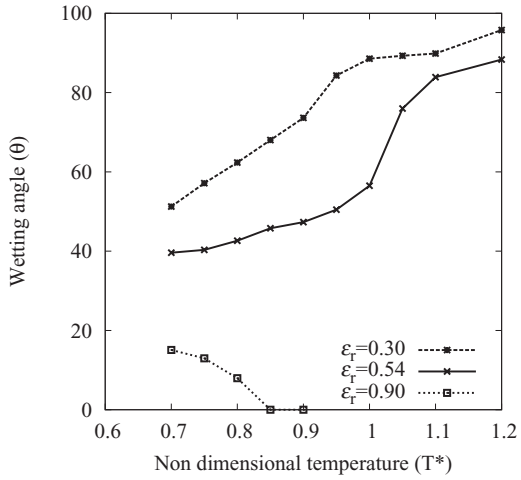

FIG. 7. Variation in wetting angle with temperature.

A contrasting behavior is observed at $\varepsilon_r = 0.90$. When T* increases, it results in better wetting, forming a thin liquid film near the solid wall. This is because the solid-liquid interaction potential is almost equal to that of liquid and this interaction potential is significant enough to arrest the liquid molecule's translatory motion to certain extent. This would result in the decreasing trend of wetting angle (θ). The above results make it clear, that the temperature of the fluid and the interaction strength of the fluid with the surface play a pivotal role in determining the wetting characteristics.

Leroy *et al.*[41] have measured the wetting angle for a cylindrical droplet on a planar solid surface for different solid-fluid interaction strength using molecular dynamics. The contact angle was computed from the mass density profiles. However, this work was based on shifted force model with a cut-off radius of $r_c = 3.82\sigma$. A comparison of this result with the present work for a temperature T*=0.9 is shown in Fig. 8. Similar trend is observed even though there exists differences in the modeling parameters.

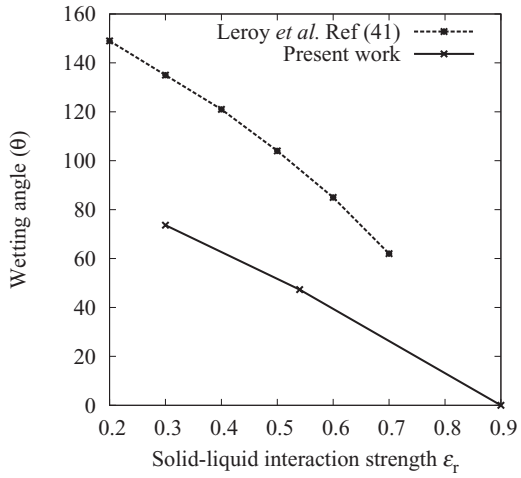

FIG. 8. Variation in wetting angle with interaction strength.

TABLE III. Simulation details for nanoparticles.

Sl. No	d*	d+Δd*	d−Δd*	Number of solid atoms
1	5.882	5.897	5.868	249
2	11.765	11.766	11.764	2123
3	17.647	17.648	17.646	7011
4	23.529	23.530	23.528	16757
5	29.411	29.412	29.410	32565

2. Spherical nanoparticle-fluid interface

For investigating interfacial tension on spherical surfaces, nanoparticles of varying diameters were used. The particle-fluid system is contained in a cubic simulation box for the different nanoparticle clusters. The details of simulation parameters are presented in Table III, while the geometric model is shown in Fig. 9.

The solid nanoparticle is obtained from a spherical cut of a fcc lattice. This spherical cluster (nanoparticle) of solid atoms (red color in Fig. 9) was embedded in a LJ monoatomic fluid (blue color). The position of the nanoparticle is fixed at the center of the simulation cell and its translation is arrested.

Following the test area method, the perturbed areas (both increased and decreased areas) are calculated and used for determining solid-liquid interfacial tension. The calculations for γ_{sl} are done with the assumption that Eq. (2) is valid for curved surfaces. Table III shows the diameter of the nanoparticles used and the number of atoms for each case. The change in diameter required for the simulations to estimate interfacial tension(γ_{sl}*) is also provided.

Figure 10 shows the variation of γ_{sl}* (for $\varepsilon_r = 0.54$) with temperature T* for various diameters. The values of interfacial tension for all the cases are found to be negative (γ_{sl}* < 0) indicating a strong wetting interaction of particle surface with liquid molecules. The figure also shows that the γ_{sl}* values are lower for smaller diameters until T* = 1.1. As T* increases beyond 1.1, the trend is found to be reversing. To illustrate this further, the variation of γ_{sl}* with diameter for different T* is analyzed and is shown in Fig. 11.

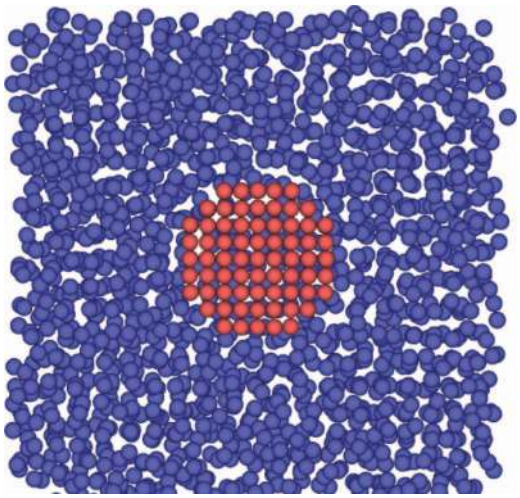

FIG. 9. Nanoparticle fluid system.

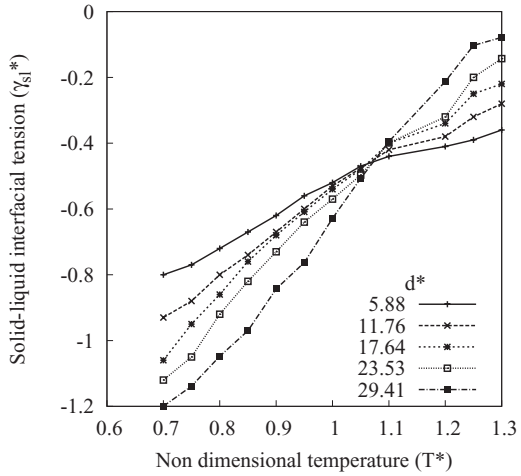

FIG. 10. Variation of interfacial tension (γ_{sl}*) with temperature T* and $\varepsilon_r = 0.54$.

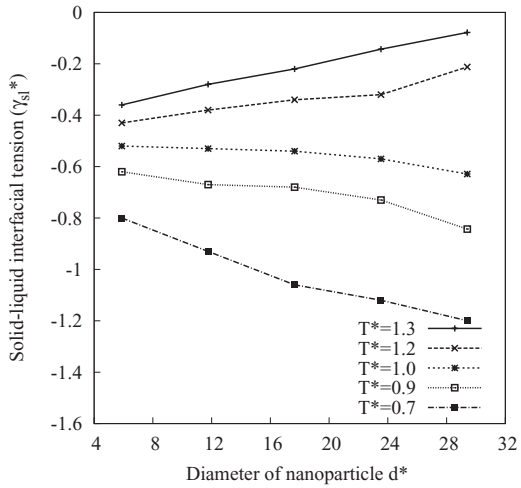

FIG. 11. Variation of interfacial tension (γ_{sl}*) with diameter for different T* and $\varepsilon_r = 0.54$.

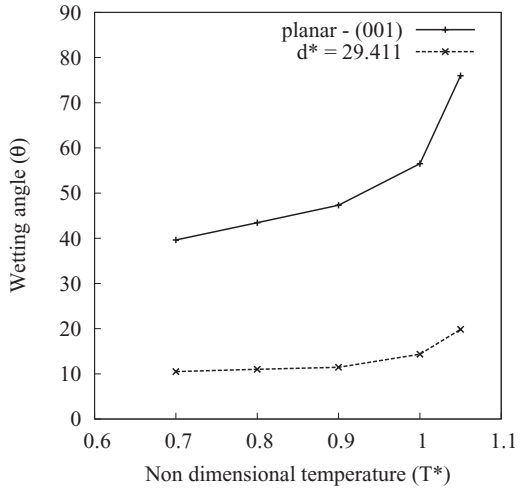

FIG. 12. Comparison of variation in wetting angle (θ) with temperature T* for planar and spherical interface ($\varepsilon_r = 0.54$).

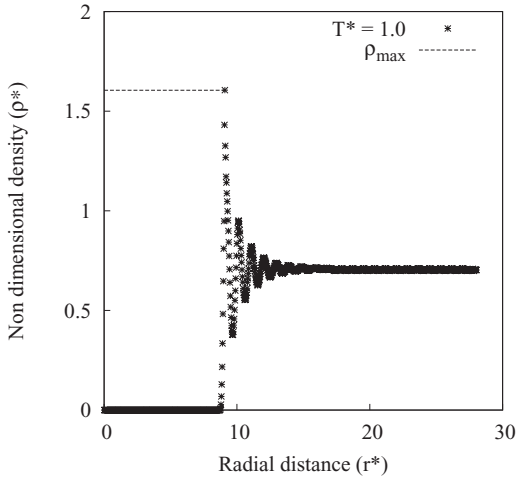

FIG. 13. Density profile of the Lennard-Jones fluid around nanoparticle at T* = 1 ($\varepsilon_r = 0.54$).

From Fig. 11, it is clear that, when particle diameter increases there is an increase in magnitude of γ_{sl}* value (for $\varepsilon_r = 0.54$). This is evident for T* values between 0.7 and 1.0. This shows an increase in wetting with the particle diameter. However, for T* greater than 1.0, γ_{sl}* reduces with further increase in particle diameter thereby showing a reverse trend. This means as temperature and diameter of particle increases, wetting behavior reduces.

In addition to the above results, a comparison of the variation in wetting angle with temperature is plotted for a nanoparticle with d* = 29.411 and for the planar case. This is shown in Fig. 12. The results indicate that as T* increases there is a rapid decrease in wetting, for planar interface, while for the spherical nanoparticle, the wetting angle increases gradually and the liquid adheres to the nanoparticle.

Figure 13 shows the density profile of the liquid around the nanoparticle of diameter d* = 17.647 (radius r* = 8.823). A peak value for the fluid density (ρ_{max}) is observed around the nanoparticle.

Figure 14 shows the variation of ρ_{max} with particle diameter for different fluid temperatures. At higher temper-

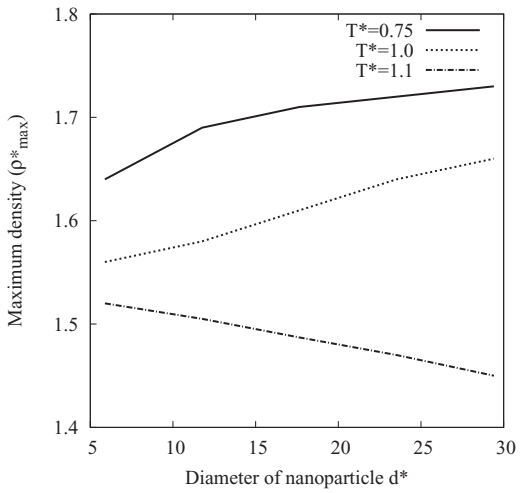

FIG. 14. Variation of peak density value of liquid with diameter ($\varepsilon_r = 0.54$).

TABLE IV. Variation in maximum density value of liquid on planar solid surface.

(001) planar interface	
T*	ρ_{max}
0.7	1.49
1.0	1.44
1.1	1.36

atures (T*>1.0) the peak density value (ρ^*_{max}) decreases when the diameter of nanoparticle increases. This means that for higher temperatures, nanoparticles with smaller diameter can retain a more ordered layer of fluid in its neighborhood compared to larger diameter nanoparticles. This layering can strongly influence the interfacial tension and hence smaller nanoparticles will have higher γ_{sl}* values, at higher temperatures.

Table IV shows the corresponding variation in maximum density values for a (001) crystallographic plane. The data indicates that peak values are much lower for planar interface when compared to spherical interfaces.

C. Comparison of interfacial tension values

Figure 15 shows the various γ* values - for vapor-liquid and solid-liquid interfaces (planar and spherical). The values of solid-liquid interfacial tension for a nanoparticle-fluid system are found to be higher than the planar surface-fluid system. For planar surface-fluid system, γ_{sl}* reaches zero as T* reaches a value of around 1.23, while it is non-zero for nanoparticle-fluid system (for $\varepsilon_r = 0.54$). This indicates that fluid around nanoparticle still remains in liquid state and does not undergo a phase change. Compared to a planar solid surface, nanoparticles thus possess an increased ability to retain a highly ordered layer of fluid molecules in its neighborhood (Fig. 13).

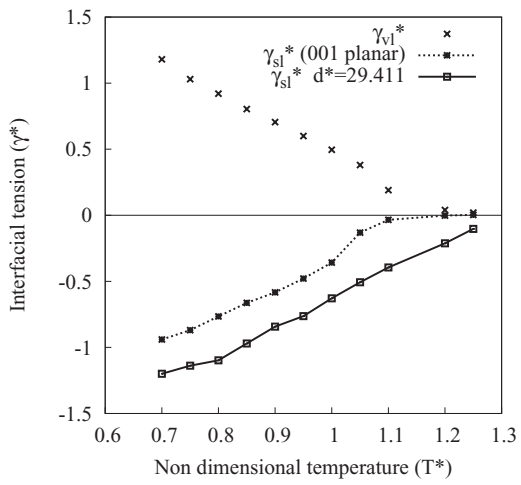

FIG. 15. Comparison of γ* values for vapor-liquid and solid-liquid interfaces.

IV. CONCLUSION

Estimation of solid-liquid interfacial tension (γ_{sl}) which plays a key role in various phenomena such as nucleation and boiling is analyzed. TASM is utilized to calculate the interfacial tension. Molecular dynamics was used to apply this methodology for two cases—one for solid-liquid planar interface and the other for the spherical nanoparticle-liquid interface.[42–44] The results show that the values of solid-liquid interfacial tension are found to be higher for nanoparticles compared to planar surface. This proves that a strong wetting interaction exists between nanoparticle and liquid molecules. This could be a factor responsible for the liquids to sustain higher heat flux without undergoing a phase change around the nanoparticle. The effect of nanoparticle size and system temperature was also studied on the interfacial tension. The study shows that γ_{sl} is a size and temperature dependent property. For lower temperatures, as diameter increases, γ_{sl} increases but a reverse trend is observed with increase in temperature. The ability of smaller nanoparticles to retain a well structured layer of fluid molecules around it even at higher temperatures is considered to be the reason for this phenomenon. The effect of curvature induced pressure in its immediate neighborhood could be the reason for the well ordered fluid layering around nanoparticles. Also that higher heat input is necessitated to break the interaction strength of fluid molecules around the spherical nanoparticle, which makes it possible to have fluid remain at liquid state.

[1]H. K. Christenson and P. M. Claesson, Adv. Colloid Interface Sci. **91**, 391 (2001).
[2]P. Attard, Adv. Colloid Interface Sci. **104**, 75 (2003).
[3]Z. Ge, D. G. Cahill, and P. V. Braun, Phys. Rev. Lett. **96**, 186101 (2006).
[4]M. Hu, H. Petrova, and G. V. Hartland, Chem. Phys. Lett. **391**, 220 (2004).
[5]E. E. Meyer, K. J. Rosenberg, and J. Israelachvili, Proc. Natl. Acad. Sci. U.S.A. **103**, 15739 (2006).
[6]J. N. Israelachvili, *Intermolecular and Surface Forces*, 3rd ed. (Academic, 2011).
[7]Y. Dou, L. V. Zhigilei, N. Winograd, and B. J. Garrison, J. Phys. Chem. A **105**, 2748 (2001).
[8]Y. Dou, L. V. Zhigilei, Z. Postawa, N. Winograd, and B. J. Garrison, Nucl. Instrum. Methods Phys. Res. B **180**, 105 (2001).
[9]S. Merabia, S. Shenogin, L. Joly, P. Keblinski, and J.-L. Barrat, Proc. Natl. Acad. Sci. U.S.A. **106**, 15113 (2009).
[10]S. Merabia, P. Keblinski, L. Joly, L. J. Lewis, and J.-L. Barrat, Phys. Rev. E **79**, 021404 (2009).
[11]S. Sinha, J. B. Freund, and V. K. Dhir, in *Proceedings of 2001 ASME Summer Heat Transfer Conferences* (ASME, 2001), Vol. 369, p. 79.
[12]S. Sinha, V. K. Dhir, B. Shi, J. B. Freund, and E. Darve, in *Proceedings of 2003 ASME Summer Heat Transfer Conferences* (ASME, 2003), Vol. 2003, p. 711.
[13]B. Shi, S. Sinha, and V. K. Dhir, J. Chem. Phys. **124**, 204715 (2006).
[14]J. G. Kirkwood and F. P. Buff, J. Chem. Phys. **17**, 338 (1949).
[15]K. Binder, Phys. Rev. A **25**, 1699 (1982).
[16]A. W. Adamson and A. P. Gast, *Physical Chemistry of Surfaces*, 6th ed. (Wiley, 1997).
[17]J. S. Rowlinson and B. Widom, *Molecular Theory of Capillarity* (Dover, 2003).
[18]G. J. Gloor, G. Jackson, F. J. Blas, and E. de Miguel, J. Chem. Phys. **123**, 134703 (2005).
[19]J. R. Errington and D. A. Kofke, J. Chem. Phys. **127**, 174709 (2007).
[20]C. Vega and E. de Miguel, J. Chem. Phys. **126**, 154707 (2007).
[21]R. Bahadur, L. M. Russell, and S. Alavi, J. Phys. Chem. B **111**, 11989 (2007).
[22]R. Bahadur and L. M. Russell, Aerosol Sci. Technol. **42**, 369 (2008).
[23]J. Mittal and G. Hummer, Faraday Discuss. **146**, 341 (2010).

[24]M. P. Allen and S. J. Tildesley, *Computer Simulation of Liquids*, 1st ed. (Clarendon, 1986).
[25]J. E. Finn and P. A. Monson, Phys. Rev. A **39**, 6402 (1989).
[26]B. Smit, J. Chem. Phys. **96**, 8639 (1992).
[27]J. J. Nicolas, K. Gubbins, W. Streett, and D. Tildesley, Mol. Phys. **37**, 1429 (1979).
[28]M. Mecke, J. Winkelmann, and J. Fischer, J. Chem. Phys. **107**, 9264 (1997).
[29]R. J. Sadus, *Molecular Simulation of Fluids*, 1st ed. (Elsevier Science, 1999).
[30]A. Trokhymchuk and J. Alejandre, J. Chem. Phys. **111**, 8510 (1999).
[31]H. Watanabe, N. Ito, and C.-K. Hu, J. Chem. Phys. **136**, 204102 (2012).
[32]S. Nosé, J. Chem. Phys. **81**, 511 (1984).
[33]S. Nosé, Mol. Phys. **52**, 255 (1984).
[34]N. B. Wilding, Phys. Rev. E **52**, 602 (1995).
[35]K. K. Mon and K. Binder, J. Chem. Phys. **96**, 6989 (1992).
[36]N. B. Wilding and A. D. Bruce, J. Phys.: Condens. Matter **4**, 3087 (1992).
[37]A. Z. Panagiotopoulos, Int. J. Thermophys. **15**, 1057 (1994).
[38]J. J. Potoff and A. Z. Panagiotopoulos, J. Chem. Phys. **109**, 10914 (1998).
[39]E. A. Guggenheim, J. Chem. Phys. **13**, 253 (1945).
[40]S. G. Kandlikar and M. E. Steinke, Int. J. Heat Mass Transfer **45**, 3771 (2002).
[41]F. Leroy and F. Muller-Plathe, J. Chem. Phys. **133**, 044110 (2010).
[42]J. Haile, *Molecular Dynamics Simulation Elementary Methods*, 1st ed. (Wiley, 1991).
[43]S. Plimpton, J. Comput. Phys. **117**, 1 (1995).
[44]W. Humphrey, A. Dalke, and K. Schulten, J. Mol. Graphics **14**, 33 (1996).